frontiers | Frontiers in Earth Science

TYPE Original Research
PUBLISHED 14 September 2023
DOI 10.3389/feart.2023.1225131

OPEN ACCESS

EDITED BY
Ali Abedini,
Urmia University, Iran

REVIEWED BY
Linda Stalker,
Commonwealth Scientific and Industrial Research Organisation (CSIRO), Australia
Angela Goodman,
National Energy Technology Laboratory (DOE), United States

*CORRESPONDENCE
Mahmoud Leila,
mahmoud_lotfy@mans.edu.eg

RECEIVED 18 May 2023
ACCEPTED 04 September 2023
PUBLISHED 14 September 2023

CITATION
Alanazi A, Al-Yaseri A, Mowafi M, Leila M and Hoteit H (2023), First assessment of hydrogen/brine/Saudi basalt wettability: implications for hydrogen geological storage.
Front. Earth Sci. 11:1225131.
doi: 10.3389/feart.2023.1225131

First assessment of hydrogen/brine/Saudi basalt wettability: implications for hydrogen geological storage

Amer Alanazi[1], Ahmed Al-Yaseri[2], Mahmoud Mowafi[1], Mahmoud Leila[3]* and Hussein Hoteit[1]

[1]Physical Science and Engineering Division, King Abdullah University of Science and Technology (KAUST), Thuwal, Saudi Arabia, [2]Center of Integrative Petroleum Research (CIPR), College of Petroleum Engineering and Geoscience, King Fahd University of Petroleum and Minerals, Dhahran, Saudi Arabia, [3]Faculty of Science, Mansoura University, Mansoura, Egypt

Introduction: Underground hydrogen (H_2) storage is a prominent technique to enable a large-scale H_2-based economy as part of the global energy mix for net-zero carbon emission. Recently, basalts have gained interest as potential caprocks for subsurface H_2 storage due to their low permeability, vast extension, and potential volumetric capacity induced by structural entrapment of the buoyant H_2. Wettability represents a fundamental parameter which controls the capillary-entrapment of stored gases in porous media.

Methods: The present study evaluates the wettability of basalt/H_2/brine system of two basalt samples from Harrat Uwayrid, a Cenozoic volcanic field, in Saudi Arabia. The H_2/basalt contact angle was measured using a relevant reservoir brine (10% NaCl) under storage conditions of 323K temperature and pressure ranges from 3 to 28 MPa using the modified sessile drop method. The surface roughness of the basaltic rocks was determined to ensure accurate results.

Results: The investigated Saudi basalt samples are water-wet, thereby they did not achieve a 100% hydrogen wetting phase even at 28 MPa pressure. The measured contact angles slightly decrease as pressure increases, thereby pressure did not significantly influences the height of the H_2 column.

Discussion: We interpret this trend to the slight increase in H_2 density with increasing pressure as well as to the olivine-rich mineralogical composition of the Saudi basalt. Thus, from the wettability aspects, Saudi basalt has the potential to store a large volume of H_2 (>1,400 m height) and maintain its excellent storage capacity even in deep, high-pressure regimes. This study demonstrates that the basalt rock texture (pore throat radii) and mineralogy control their capacity for subsurface H_2 storage.

KEYWORDS

hydrogen, Saudi basalt, Harrat Uwayrid, wettability, seal integrity, subsurface storage

1 Introduction

Global efforts are underway to reduce harmful anthropogenic emissions of greenhouse gases such as carbon dioxide (CO_2) by adopting strict environmental regulations and transitioning toward a diversified energy mix instead of complete reliance on fossil fuels (IEA, 2018; Hashemi et al., 2021; Alanazi et al., 2023a). Hydrogen (H_2) emerges as a

promising clean fuel to support decarbonization by converting energy production from fossil fuels into a more efficient and environmental-friendly form, thus supporting the transition into renewable and sustainable resources (McCollom and Bach, 2009; Prinzhofer et al., 2018; Pan et al., 2021; Leila et al., 2022; Alanazi et al., 2023b). However, a wide-scale implementation of an H_2-based economy requires a medium of giga-to tera-scale storage capacity, which is theoretically associated with specific geological contexts such as saline aquifers, depleted oil and gas reservoirs, and salt caverns (e.g., Tarkowski, 2019; Heinemann et al., 2021). Successful industrial-scale H_2 geological storage has been implemented in salt caverns due to their impervious characteristics and perfect seal integrity (Michalski et al., 2017; Al-Mukainah et al., 2022).

Sedimentary formations with existing infrastructures such as depleted reservoirs have attracted attention for subsurface storage due to their efficient pore system, storage, and sealing capacities (Pfeiffer et al., 2017; Yekta et al., 2018; Tarkowski, 2019; Alanazi et al., 2022c). Furthermore, volcanic basaltic rocks have recently been recognized as an unconventional storage medium and a potential rival to sedimentary formations (Iglauer et al., 2020). Basaltic rocks often exist vastly on the continents in the form of extensive dykes and sills. They also cover approximately two-thirds of the oceanic crust (Gislason and Oelkers, 2014; Matter et al., 2016). Therefore, various efforts started to investigate their suitability for CO_2 storage in terms of pore system, permeability, trapping mechanisms, and sealing efficiency (Gislason et al., 2010; Iglauer et al., 2020). However, the efficacy of basaltic rocks for H_2 storage still need further investigation.

The primary trapping mechanisms are structural/residual trapping, dissolution, and mineralization trapping (Bui et al., 2018). The latter has shown a CO_2 mineralization in basalt within time scales superior to those predicted for clastic sedimentary rocks (White et al., 2020). However, for H_2 subsurface storage, the residual and structural trapping mechanisms are more pronounced. In contrast to the hydrogen storage being cyclic in nature, it might be worth emphasizing the permanent nature of CO_2 storage for contrast (Ma et al., 2019; Alanazi et al., 2022a; Alanazi et al., 2022c; Ali et al., 2022b; Alanazi et al., 2023c). In addition, H_2 storage requires a cushion gas (e.g., CO_2, N_2, and CH_4) to remain in place and maintain the hydrostatic pressure of the reservoir (Kanaani et al., 2022).

The wettability of basalt/gas/brine is a crucial parameter controlling the trapping efficiency of the buoyant gas beneath a caprock (Hosseini et al., 2022c). The flow behaviour and interfacial characteristics of H_2-brine in the subsurface differ from CO_2 and CH_4 (Chow et al., 2018). The interfacial tension between rock and gas plays a significant role in gas storage within the pore system. Therefore, the gas-rock wettability is a critical parameter in understanding the rock's capability for entrapment. Wettability controls the gas flow and migration within a rock pore structure, affecting storage capacity and sealing efficiency (Blunt, 2016; Ali et al., 2022a). While basalt/CO_2/brine wettability studies are available with limited testing conditions (Iglauer et al., 2020; Abdulelah et al., 2021; Al-Yaseri et al., 2021b), there is a noticeable lack of studies on basalt/H_2 wettability limited to two studies; one theoretical and another experimental (Table 1). Al-yaseri et al. (2021a) and Al-Yaseri et al. (2021b) developed empirical correlations using contact angle measurements and densities of helium (He), carbon dioxide (CO_2), nitrogen (N_2), methane (CH_4), and argon (Ar) to predict the three-phase contact angles of basalt/H_2/brine at the same conditions (Al-Yaseri and Jha, 2021). While, Hosseini et al. (2022a) reported experimental measurements of contact angles for basalt using the tilted plate method at two temperatures (308 and 343K) and varying pressure from 5 to 20 MPa. Previous studies that tackled the basalt/H_2 wettability measurements outlined a weak to intermediate water-wet behaviour for the basalt at elevated levels of pressure and temperature. This behaviour would be beneficial for storing thick hydrogen columns in the subsurface.

The present study provides an experimental investigation of the H_2/brine wettability of two basalt samples collected from the Cenozoic Harrat Uwayridh volcanic field in the northwest of Saudi Arabia (Figure 1). The basalt wettability was measured at various geological storage conditions to explore their potential for subsurface H_2 storage. In theory, thick basaltic rocks can provide good sealing properties for H_2 storage in the underlying clastic reservoirs (Hosseini et al., 2022a). Basaltic rocks' capillary sealing efficiency and storage capacity are significant characteristics to be tested. Accordingly, the sealing efficiency represented by capillary entry pressure and maximum static H_2 column should be calculated to assess the storage feasibility using basalt rocks' typical pore sizes (Duncan and Al-Amri, 2013; Espinoza and Santamarina, 2017; Alanazi et al., 2022a; Alanazi et al., 2022b; Ali et al., 2022b; Alanazi et al., 2022c).

2 Materials and methods

2.1 Basaltic samples

Two Saudi basaltic samples were collected from Harrat Uwayrid, a Cenozoic volcanic field in the Medina region, NW Saudi Arabia, Figure 1 (Duncan and Al-Amri, 2013). The Harrat Uwayrid comprises an elongate NW-SE oriented volcanic field of a strongly eroded basaltic plateau extending over approximately 230 km^2. The Harrat Uwayrid basalt overlies above the Cambrian continental sandstones of the Siq Formation (Coleman et al., 1983; Altherr et al., 2019). The age of Harrat Uwayrid basalts ranges from Miocene to Quaternary, contemporaneous with the several episodes of volcanic activities in Arabia (Kaliwoda et al., 2007). The Miocene basalt is strongly eroded and consists mainly of alkali olivine basalt, whereas the younger Quaternary basalt contains mantle xenoliths and megacrysts (Altherr et al., 2019). The samples were selected from two locations north and south of the elongated volcanic field. The investigation aims to study the efficiency of Harrat Uwayrid basaltic rocks as a seal and evaluate potential hydrogen storage in the underlying Cambrian sandstone formation for a practical period of time.

2.2 Sample characterization

2.2.1 X-ray diffraction and scanning electron microscopy

Whole-rock X-ray diffraction (XRD) analysis was conducted on the Saudi basalt samples. The samples were powdered and measured for XRD using a Bruker-D8 Advance diffractometer (Bruker AXS

TABLE 1 Summary of wettability investigations of basalt/CO_2/brine systems.

References	Basalt source	Pressure, MPa	Temperature, K, ˚C	Brine salinity, wt%	Main findings
Iglauer et al. (2020)	CarbFix, Hellisheidi geothermal area, Southwest Iceland	5–17	308.15 K (35 ˚C) and 333.15 K (60 ˚C)	4% NaCl, 4% $CaCl_2$, 1% $MgCl_2$, and 1% KCl	The contact angle increases with pressure and decreases with temperature. Basalt showed an intermediate water-wet to weakly CO_2-wet similar to sedimentary caprocks linked to the similarity in elemental composition and total organic carbon (TOC)
Al-Yaseri et al. (2021a)		5–20	323 K (~50 ˚C)	0.3 Molality NaCl	Contact angle increases with pressure, and SiO_2 nanoparticles turn the CO_2-wet basalt surface into weakly water-wet
Abdulelah et al. (2021)		4–20	308 K (35 ˚C) and 333 K (60 ˚C)	4% NaCl, 4% $CaCl_2$, 1% $MgCl_2$, and 1% KCl	Basalt's CO_2 sealing capacity is reduced as the contact angle (pressure) and temperature increases
Al-Yaseri et al. (2021b)	Western Australia (WA) basalts	0.1–20	298 and 323 K (~25˚C–50 ˚C)	Deionized water and ultra-pure NaCl salt	Basalt turned from water-wet, into an utterly CO_2 wet with pressure

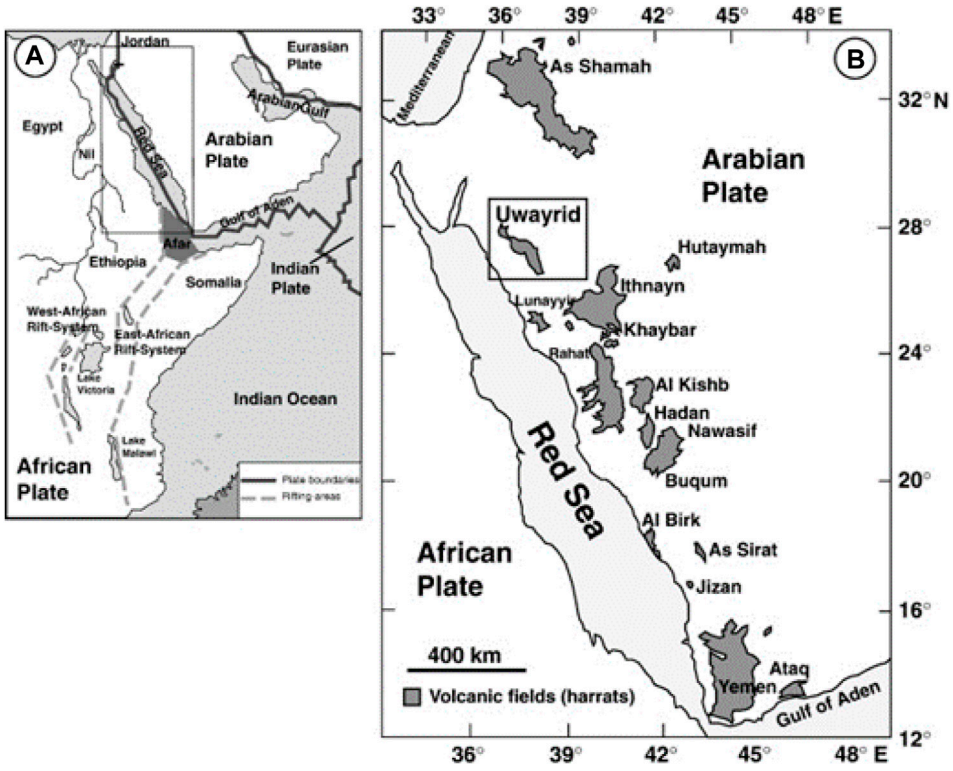

FIGURE 1
Harrat volcanic fields on the Arabian peninsula shown the tectonic map of the Arabian shield **(A)** and **(B)** a map of Harrat Uwayridh and neighbouring plates, adopted from Altherr et al. (2019).

GmbH, Karlsruhe, Germany). The measurement comprised a step scan in the Bragg-Brentano geometry having a CuKα radiation of 40 kV and 40 mA to measure XRD peaks. The XRD peak interpretation was performed using Bruker-EVA software and peak comparison with the International Centre for Diffraction Data (ICCD) standard database.

The SEM analysis was performed on the two Harrat Uwayrid basalt samples using JEOL's JSM-7001F Schottky SEM. Polished sections from the basalt samples were first mounted on aluminium stubs. The mounted sections were then coated with gold before the SEM analysis.

2.2.2 Fourier transform infrared spectroscopy (FTIR)

The spectra of Fourier Transform Infrared Spectroscopy (FTIR) are sensitive to variations in mineralogy and crystal structure, and

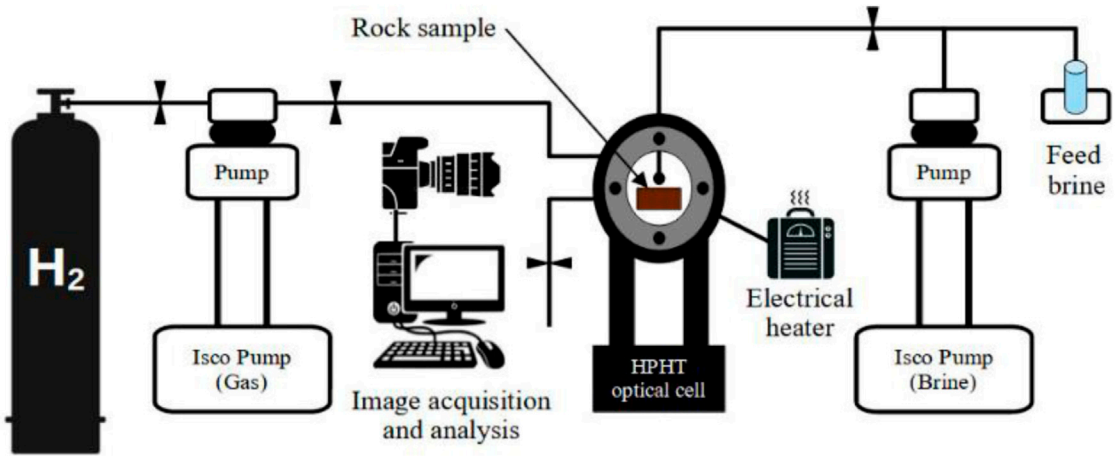

FIGURE 2
Schematic experimental design for the contact angle measurements of H_2/basalt/brine systems.

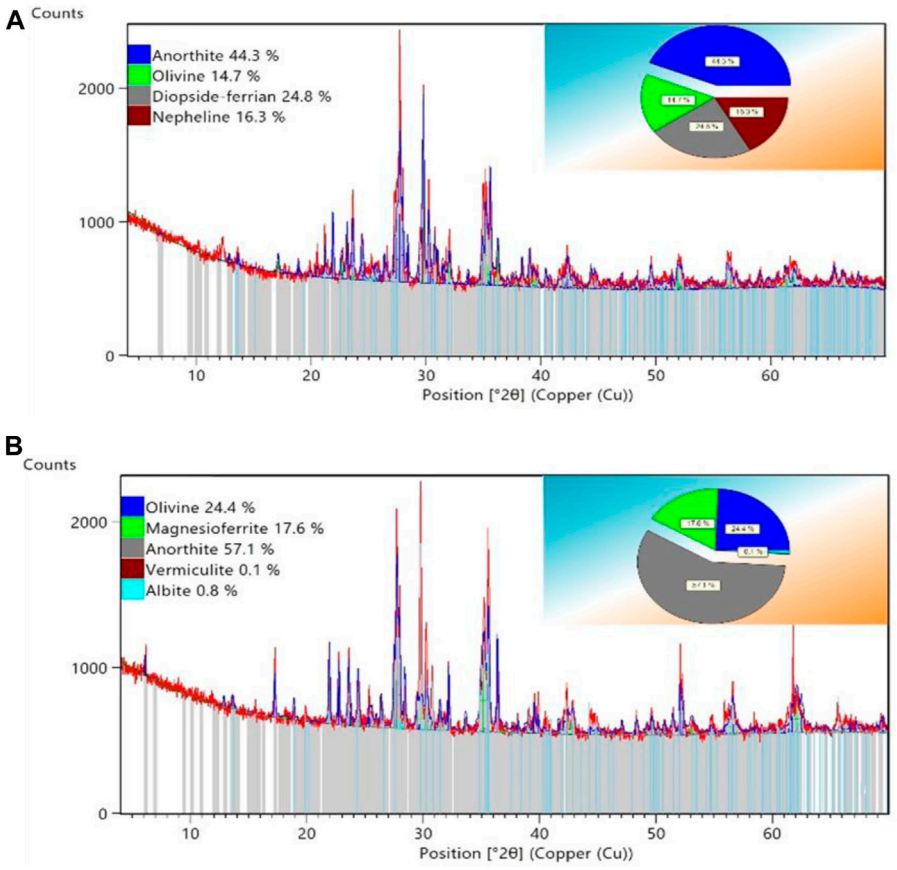

FIGURE 3
Interpreted XRD patterns illustrating the mineralogical composition of the studied Saudi basalt 1 **(A)** and 2 **(B)**.

therefore they are qualitatively utilized to identify the mineral phases in the samples based on their crystal structure. FTIR determines the absorption wavelengths related to the molecular excitation states of covalent bonds in the composition of the samples (Mbonyiryivuze et al., 2015). FTIR spectra for the Saudi basalt samples were obtained utilizing a Bruker TENSOR-27 FTIR spectrometer containing a source of infrared waves, a beam splitter, and equipped with a susceptible DigiTectTMdetector system. Approximately 0.5 mg of

TABLE 2 A comparison of XRD quantitative analysis results of the bulk mineralogy for the Saudi basalt samples compared to the mineral compositions of the previously analyzed basalt samples for wettability and underground gas storage.

Sample	Mineral phases	Abundance (%)	Study
Saudi basalt 1	Anorthite	44.3	This work
	Olivine	14.7	
	Diopside-ferrian	24.8	
	Nepheline	16.3	
Saudi basalt 2	Anorthite	57.1	This work
	Olivine	24.4	
	Magnesioferrite	17.6	
	Albite	0.8	
Iranian basalt	Anorthite	55	Hosseini et al. (2022a)
	Augite	25	
	Orthoclase	16	
	Lizardite	4	
Icelandic basalt 1	Labradorite	29.30	Abdulelah et al. (2021)
	Augite, Antarctica	18.25	
	Montmorillonite	2.30	
	Volcanic glass	50.15	
Icelandic basalt 2	Labradorite	58.6	Al-Yaseri et al. (2021a)
	Augite	36.5	
	Montmorillonite	4.6	
	Quartz	0.3	
Western Australia (WA) basalt	Labradorite	58.6	Al-Yaseri et al. (2021b)
	Anorthite	21.3	
	Augite	18.9	
	Nontronite	<1	
	Ilmenite	<1	

the powdered samples were mounted in metal disks, then dispersed in 200 mg of KBr before heating at 120 °C to release the absorbed water. The samples were scanned in the wavenumber region of 4,000–400 cm^{-1} to obtain the FITR spectra.

2.2.3 Total organic carbon (TOC) analysis

The total organic carbon (TOC) content in the two Saudi basalt samples was measured using Rock-Eval pyrolysis 7S (©Vinci Technologies). The apparatus is equipped with an oven allowing a high-temperature pyrolysis and air oxidation of approximately 10 mg of the powdered basalt samples. The oven temperature rates were adjusted from 0.1°C to 50°C/mn, with a 0.1 °C step.

2.2.4 Surface roughness measurement

The surface roughness of a sample can significantly affect the wettability and, in turn, the contact angles of the H_2/brine/basalt system (AlRatrout et al., 2018; Mehmani et al., 2019). It has been reported that the irregularity of a solid surface or surface roughness is directly linked to the hydrophobicity status of that solid caused by fluids entrapment in the surface's depressions (Morrow, 1975; Yen, 2015; Li et al., 2022). Thus, the surface roughness of Saudi basalt samples was measured using a surface roughness analyzer (KRÜSS GmbH, Germany). The KRÜSS GmbH uses the confocal microscopy technique to build a spatial schematic of the surface topography of high resolution using a rotating disk. The roughness of the selected vertical readings is provided based on the best root mean error of the multiple locations of the sample's surface.

2.3 Experimental measurement of contact angle

The contact angles were measured using the modified sessile drop method utilizing a KRÜSS fluid drop analyzer (DSA100 model) and a high-pressure and high-temperature (HPHT) optical cell (Figure 2). Pure H_2 gas (99.99 mol%) and a synthetic reservoir brine of 10 wt%

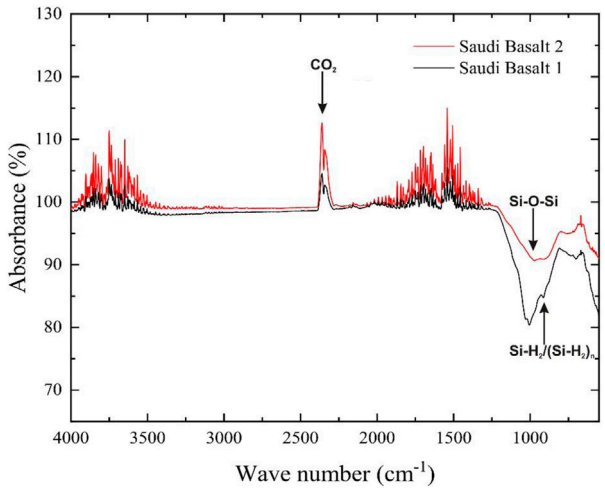

FIGURE 4
FTIR spectra of the analyzed Saudi basalt samples.

NaCl were used for the contact angle measurements at testing conditions. First, the basalt sample was cleaned with distilled water and dichloromethane, cut into 1 cm × 1 cm × 0.5 cm dimensions. Further cleaning by purging with nitrogen was conducted prior to emplacement of the samples on a horizontal plate inside a high-temperature and pressure (HTHP) cell. Then, the H_2 is injected and pressurized using an ISCO pump (500 D) of 0.001 MPa precision. The temperature is increased using an electrical heater to reach the desired temperature (323K). Afterwards, a brine droplet of 5 μL (±2 μL) is manually introduced through a needle dispenser, controlled by another ISCO pump, and released on the substrate surface. Finally, the contact angle is measured at adiabatic conditions in a continuous increment measurement where the pressure increases gradually from 3 MPa to 28 MPa, and the contact angle is measured at each pressure step. The purpose of such modified measurement from the conventional sessile drop method is to measure the hydrogen contact angle at high pressure levels which may occur in the subsurface where a continuous pressure is applied by surrounding rocks and formation fluids when H_2 is injected into the geological formation for subsurface storage. Al-Mukainah et al. (2022) have recently adopted the same modified sessile drop method (applied in this work) to measure H_2/shale/brine contact angles and evaluate potential H_2 storage in shale formations (Al-Mukainah et al., 2022). Images were acquired using a high-resolution camera to capture the drop behaviour during the experiment. The contact angle is then analyzed using KRÜSS DSA software. The contact angle measurement was repeated three times for better accuracy. The average standard deviation for the contact angle from the two samples was approximately ±3°. Before the contact angle measurement, the surface roughness of the basalt samples was determined using the Surface Roughness Analyzer (KRÜSS GmbH) (Al-Yaseri et al., 2021c).

3 Results and discussion

3.1 Characterization of Harrat Uwayrid basalt

The measured TOC values for the analyzed basalt samples (1 and 2) were approximately 0.05 wt% and 0.03 wt%, respectively, measured by Rock-Eval pyrolysis. The XRD results

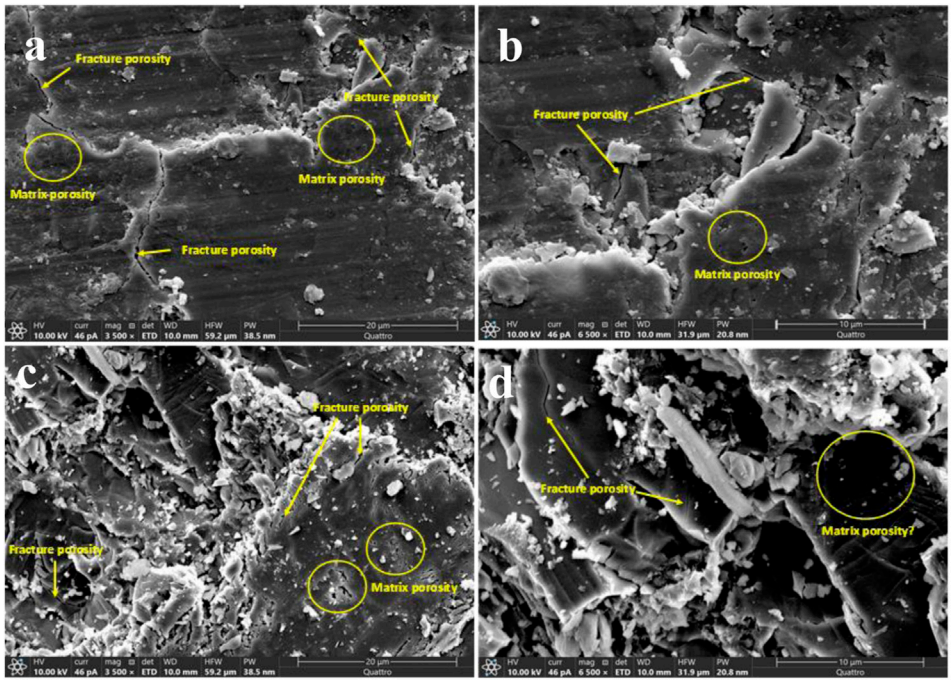

FIGURE 5
SEM microphotographs illustrating the surface morphology and textural characteristics of the studied Saudi basalt 1 **(A,B)** and 2 **(C,D)**.

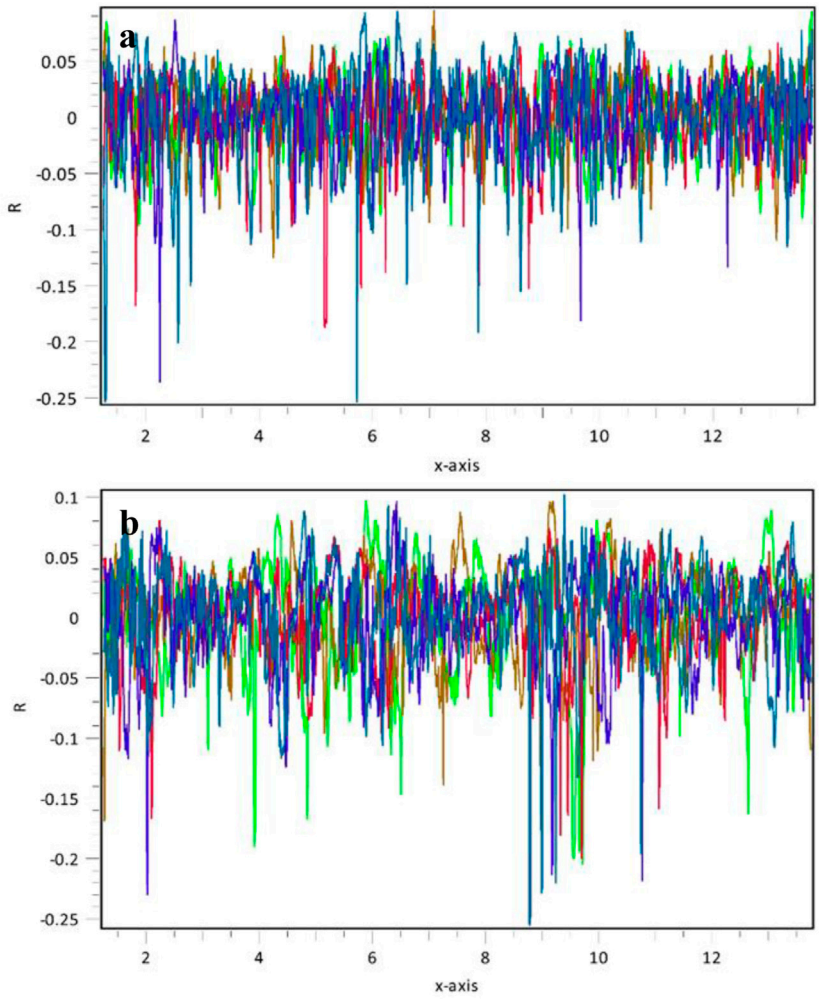

FIGURE 6
Surface roughness of Saudi basalt samples tested over 25 by 40 μm regions of each sample—**(A)** Saudi basalt 1 of 29.74 μm mean roughness and **(B)** Saudi basalt 2 of 25.14 μm mean roughness.

provide reveal a semi-quantitative mineralogy analysis (Figure 3). The analyzed samples were collected from two different locations (south and north) to evaluate any changes in the mineral composition that could potentially influence H_2/basalt/brine wettability. The XRD analysis demonstrates a similarity in the primary minerals between the two samples, dominated by anorthite and olivine of about 44.3% and 57.1% for anorthite, 14.7%, and 24.4% for olivine in the Saudi basalt 1 and 2, respectively. Clinopyroxene (diopside) and nepheline were also found only in Saudi basalt 1 (24.8% and 16.3%, respectively), while Saudi basalt 2 contains magnesioferrite (~17.6%) and traces of albite and vermiculite that were missing in Saudi basalt 1.

A mineralogical comparison between the investigated Saudi basalts and other basaltic rocks tested for underground gas storage (Table 2) reveals significant differences, which may influence the wettability measurement and storage efficiency of H_2 beneath the basalts. Relative to other basalt samples (Iranian and Icelandic basalts), Saudi basalts are enriched in olivine relative to plagioclase and alteration products (e.g., clays). Such variation in mineralogy typifies a differential alteration (Harnois, 1988; Weltje et al., 1998; Dessert et al., 2003; Leila et al., 2018; Leila et al., 2021). For example, olivine minerals are more susceptible to chemical weathering and alteration into other phases such as serpentine; thus, enrichment of olivine phases would infer into fresh and un-altered samples. Therefore, the Saudi basalts are fresh samples, whereas other basalt samples were subjected to more severe chemical alteration. Such variation in chemical alteration may impact the wettability measurements and hence the storage potential. Notably, nano-capillary pores are more common in clays and these nanopores may become saturated with hydrogen, and hence reduce the storage capability of the basaltic rock. Additionally, the occurrence of specific clay phases that are susceptible to hydro-swelling (e.g., Montmorillonite) would decrease pore throat size and pore system connectivity (Aksu et al., 2015; Jiu et al., 2021). Thereby, variation in mineralogical composition would significantly impact the capillary behaviors and sealing capacity of the naturally-impervious rocks.

The FTIR measurement indicates the dominant chemical functional groups on a rock surface, significantly contributing to the wettability status (Madhurima et al., 2011; Cheng et al., 2014;

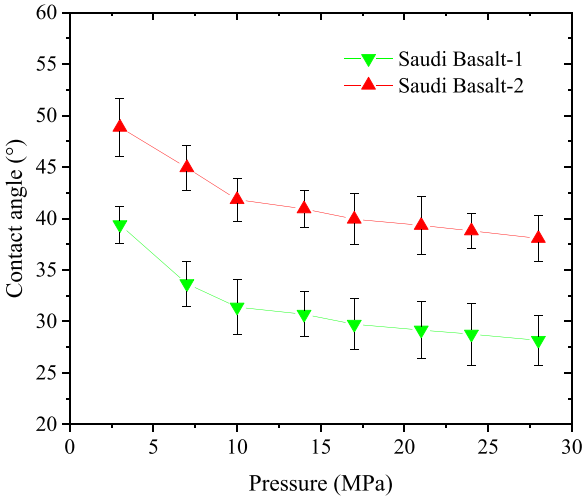

FIGURE 7
Static contact angles of H_2/brine systems on Saudi basalt samples at different pressures and constant temperature of 323K. The uncertainty bars in the plots range from 2.1° to 3.3° (with the relative standard uncertainties of 1K for temperature and 0.1 psi for pressure).

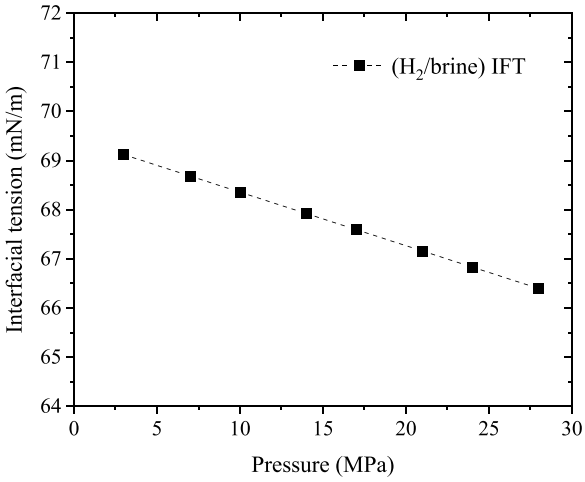

FIGURE 8
Hydrogen/brine interfacial tension at different pressures and constant temperature of 323K, extrapolated from the data in Chow et al. (2018) with ±1 mN/m uncertainty.

Pillai et al., 2018). The FTIR analysis of the Saudi basalt samples demonstrated that SiO_2 is the primary chemical group on the samples' surface (Figure 4). Visible wave numbers in the range of 1,000 and 1,200 cm^{-1} correspond to the Si-O-Si bond (OH and Choi, 2010; Waman et al., 2011; Liu et al., 2019). The interpreted Si-O-Si bond is attributed to the presence of silica and silicate minerals in the studied basalt samples. The more pronounced Si-O-Si bond in Saudi basalt 1 is most likely related to the occurrence of nepheline which is absent in basalt 2. Weak absorption at 800 cm^{-1} corresponds to Si-H_2/(Si-H_2)$_n$ band. This band is more significant in the Saudi basalt 2 sample typifying a more hydrophilic characteristics relative to basalt 1 sample (Liu et al., 2019). FTIR is also corroborated by XRD and XRF which confirmed a silica-rich samples. According to XRF data, basalts 1 and 2 contain 36.16% and 37.50% SiO_2, respectively.

The SEM analysis focuses on the basalt samples' surface morphology and micro-scale characteristics, such as the fracture and matrix porosity, which can significantly influence the wettability measurement (Rucker et al., 2019). Micro, irregular, stylolite-like fractures were found with more intensity in Saudi basalt 1 (Figures 5A, B) compared to the Saudi basalt 2 sample (Figures 5C, D). Both samples showed low matrix porosity in the micro- and nano-scales. However, matrix porosity is relatively more significant in Saudi basalt 2 sample (Figure 5D). Notably, the fracture and matrix pores are scattered and non-connected, suggesting that the studied Saudi basalts are impervious with nano-scale pore throats. The surface roughness analyzer indicated a root-mean-square (RMS) from different vertical locations of approximately 29.74 and 25.14 µm surface roughness for Saudi basalt 1 and Saudi basalt 2, respectively (Figure 6). The RMS roughness is a measure of the standard deviation in the surface heights values, thus reflecting the extent of surface irregularities (Gadelmawla et al., 2002). The surface topography of the samples induces a paramount impact on the rock-fluid contact angle. Irregular, rough surfaces with high RMS values often enhance the wetting behavior of the sample (Johnson and Dettre, 1964). Additionally, irregular surfaces usually show water-wet behavior. Nevertheless, the influence of the surface roughness becomes insignificant below 1,000 µm (Al-Yaseri et al., 2016). Thus, it does not impact the wetting characteristics of storage formation rocks (Al-Mukainah et al., 2022).

3.2 Effect of pressure on H_2/basalt/brine wettability

The static H_2/brine/basalt contact angles of the two samples were measured at different pressures up to 28 MPa and a temperature of 323K (Figure 7). The Saudi basalt 2 displayed slightly higher contact angles than Saudi basalt 1. The H_2 wettability of Saudi basalt 2 demonstrated a more hydrophilic behavior than Saudi basalt 1, mainly attributed to the Si- H_2 bond FTIR peak, which is higher in Saudi basalt 2 than Saudi basalt 1. However, the variation in contact angle measurements could be attributed only to surface roughness differences (AlRatrout et al., 2018; Mehmani et al., 2019). Nevertheless, both samples displayed a strong to intermediate water-wet behaviour and demonstrated a slight decrease in pressure, which is linked to the decline of interfacial between the brine and H_2 gas (Figure 8). Images of drop profiles are shown in Figures 9, 10 for the different pressure steps confirming the observation of the contact angle measurements. These profiles demonstrate intermediate to strongly water-wet behaviour.

Overall, the contact angles for both basalt samples displayed an initial steep drop as pressure increased from 2.5 MPa to 10 MPa, which started to level up at 10 MPa pressure. The observed decrease in the contact angles with pressure differs from some of the gas/basalt/brine measurements, for example, (Iglauer et al., 2020; Al-Yaseri et al., 2021a; Hosseini et al., 2022b), where the contact angle increase with pressure. In this work, the modified sessile drop is applied, where the contact angle is measured for each pressure step in a continuous pressure increment approach. Moreover, the

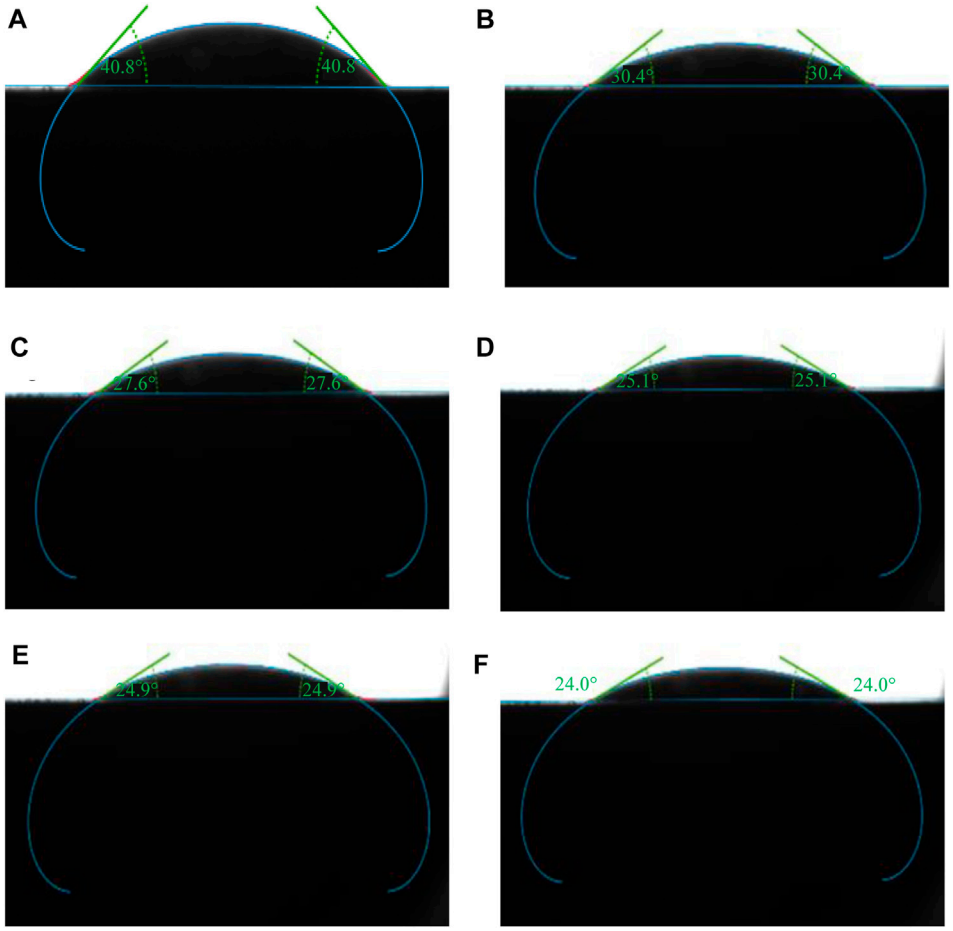

FIGURE 9
Sessile drop of brine on Saudi basalt-1 surrounded by hydrogen, measured at a constant temperature of 323K and different pressure steps **(A)** 3 MPa, **(B)** 7 MPa, **(C)** 14 MPa, **(D)** 21 MPa, **(E)** 24 MPa, and **(F)** 28 MPa.

decrease in contact angle with pressure for the H_2/basalt/brine system is related to the decline of H_2-brine interfacial tension (IFT) with increasing pressure (Figure 8) and the very low density of H_2 compared to CO_2, where the cohesive forces between gas molecules and rock matrix increase at higher pressures (Yekeen et al., 2021; Al-Mukainah et al., 2022).

3.3 H_2/brine wettability of Saudi basalt compared to Iranian basalt

The present work measured the static contact angle of H_2/basalt/brine. While the only available work of H_2/basalt/brine wettability in the literature by Hosseini et al. (2022b) was conducted using the tilted plate method, first introduced by Lander et al. (1993), and provides dynamic contact angles. The tilted plate method theoretically attempts to represent the imbibition (wetting phase displacing non-wetting) and drainage (non-wetting phase displacing wetting) processes by correlating them to tail contact angles of a brine drop on a tilted rock surface, the receding contact angle (θ_r) and advancing contact angle (θ_a).

In the literature, there is extensive experimental work applying the tilted plate method to investigate underground H_2 storage using different rock types, where the dynamic contact angles are related to the intrinsic contact angle or the equilibrium contact angle (θ_e) (Morrow, 1975; Chow et al., 2018; Liang et al., 2020; Hashemi et al., 2021; Ali et al., 2022b). The equilibrium contact angle can be calculated using Tadmore's empirical approach (Tadmor, 2004) based on Young's equation and Neumann's equation of state (Li and Neumann, 1992; Kwok and Neumann, 1999) as a function of the receding (θ_r) and advancing (θ_a) contact angles as shown in Eq. 1:

$$\theta_e = cos^{-1}\left(\frac{\aleph_a \cos\theta_a + \aleph_r \cos\theta_r}{\aleph_a + \aleph_r}\right) \quad (1)$$

Where θ_a, θ_r represent advancing and receding contact angles, and $\aleph_a$ and $\aleph_r$ are correlation parameters (receding and advancing), calculated as shown in Eqs 2, 3:

$$\aleph_a = \sqrt[3]{\left[\frac{sin^3\theta_a}{2 - 3cos\,\theta_a + cos^3\theta_a}\right]} \quad (2)$$

$$\aleph_r = \sqrt[3]{\left[\frac{sin^3\theta_r}{2 - 3cos\,\theta_r + cos^3\theta_r}\right]} \quad (3)$$

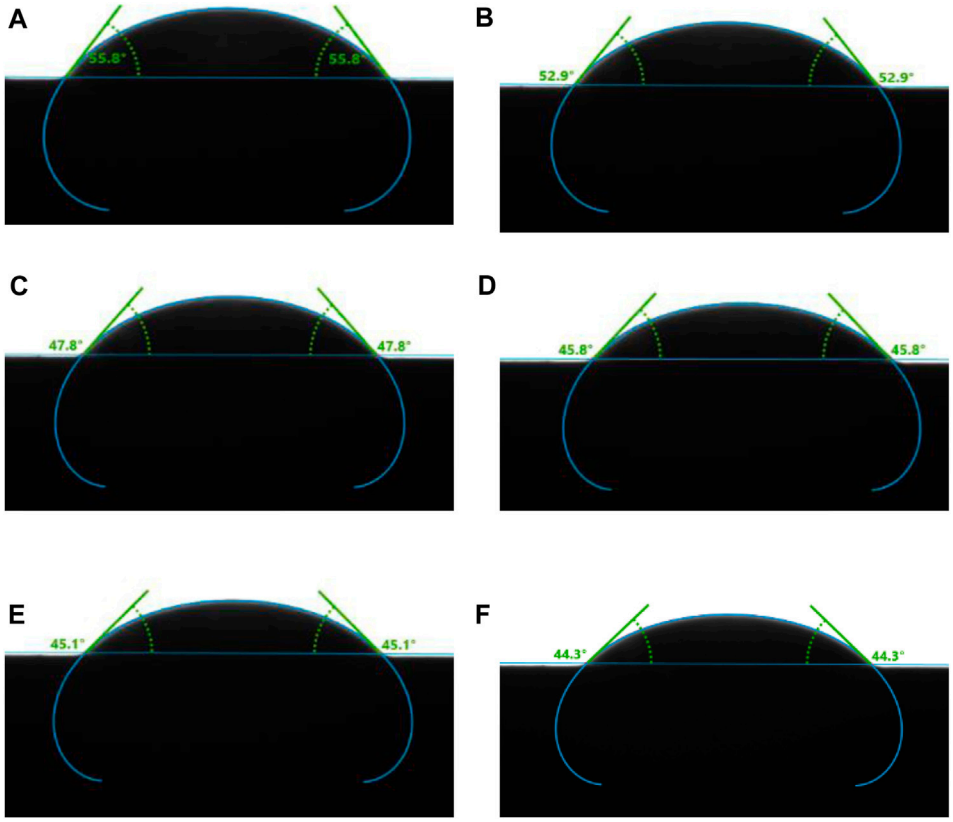

FIGURE 10
Sessile drop of brine on Saudi basalt-2 surrounded by hydrogen, measured at a constant temperature of 323K and varying pressures—**(A)** 3 MPa, **(B)** 7 MPa, **(C)** 14 MPa, **(D)** 21 MPa, **(E)** 24 MPa, and **(F)** 28 MPa.

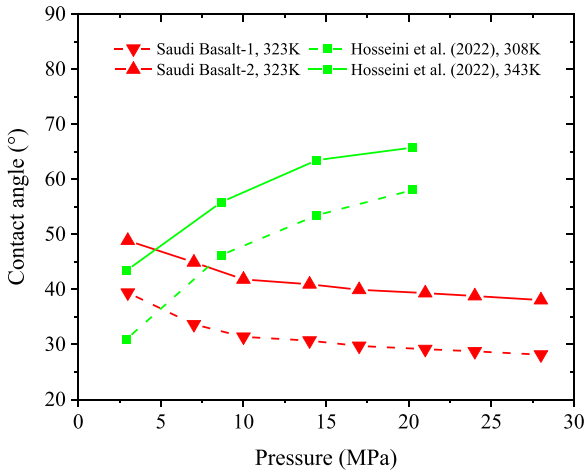

FIGURE 11
Static contact angles of H_2/brine systems of Saudi basalt samples at 323K, compared to the calculated equivalent contact angles on Iranian basalts at 308K and 343K (Hosseini et al., 2022a).

The above correlation was used to calculate θ_e from the dynamic contact angles measured at two different temperatures (308 K and 343 K) by Hosseini et al. (2022a). Then, it was used for comparison with H_2/basalt/brine static contact angles in this study, which was conducted at a temperature of 323 K (Figure 11). The comparison reveals a relatively close approximation, particularly at low pressures (less than 10 MPa). The trend of the measured contact angles differs due to the different applied experimental techniques.

The modified sessile drop used in this work depends on maintaining an isolated gas environment and measuring the change in drop contact angles at each pressure point via a subsequent increase of the pressure inside the high-pressure, high-temperature cell. In contrast, the titled-plate method measures the dynamic contact angles in a stepwise procedure involving using multiple rock samples and depressurizing the cell each step to load the new sample. Moreover, the mineralogy comparison based on XRD analysis listed in Table 2 demonstrates that the Saudi basalts have different mineral compositions than the Iranian basalt. The Iranian basalt composition contains more lizardite and plagioclase; thus, it can exhibit a wettability behaviour similar to clay-rich rocks (Abramov et al., 2019; Al-Yaseri et al., 2021c).

3.4 Capillary sealing efficiency and H_2 static column height

The sealing efficiency of a caprock is evaluated by studying capillary characteristics at the interface between the formation brine in the caprock and the injected gas. A non-wetting phase (e.g., CO_2 and H_2) cannot invade the rock until the pressure drop exceeds a certain threshold, which is known as the capillary entry pressure

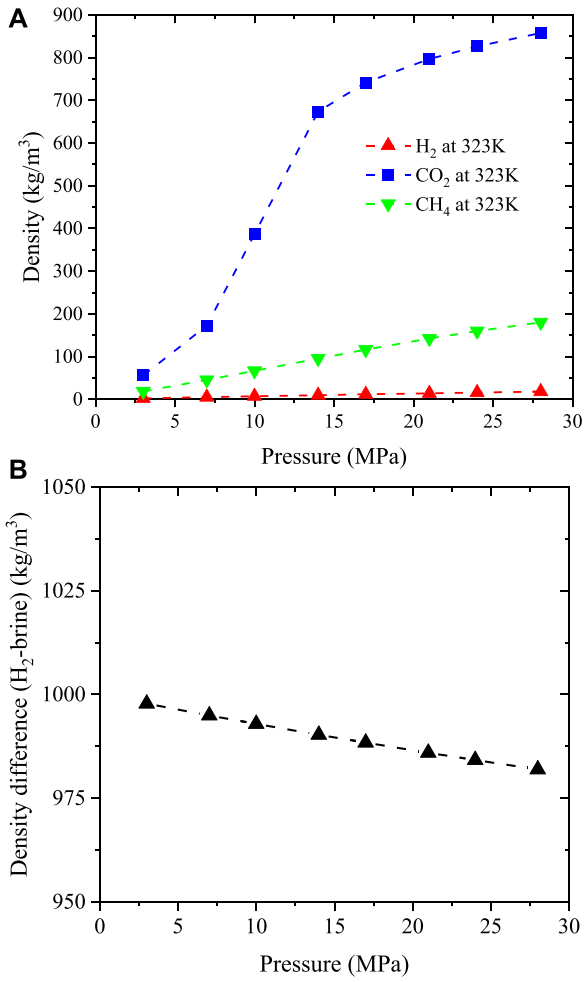

FIGURE 12
Density variation over pressure **(A)** and the density difference between 10%NaCl brine and hydrogen at varying pressure and constant temperature of 323K **(B)**. Note: the data were extracted from NIST database (Lemmon et al., 2018).

(p_{ce}) and determined by the Laplace equation (Espinoza and Santamarina, 2017), as follows:

$$p_{ce} = \frac{2\gamma_{lg}\cos\theta_g}{r} \tag{4}$$

where γ_{lg} is the brine/gas interfacial tension, and θ_g is the contact angle of the gas, and r is the effective pore throat radius of the rock.

The sealing capacity and storage efficiency of the studied basalt samples at 323K is obtained by calculating the static height of the H_2 column that can be safely trapped beneath the basaltic rocks using Eq. 5 (Dake, 1978):

$$h_g^{max} = \frac{2\gamma_{lg}\cos\theta_g}{rg(\rho_l - \rho_g)} \tag{5}$$

where h_g^{max} is the maximum static height of the column that can be safely trapped beneath the seal (Iglauer, 2022), g is the gravitational acceleration, ρ_l and ρ_g are the density of the liquid and gas phases, respectively.

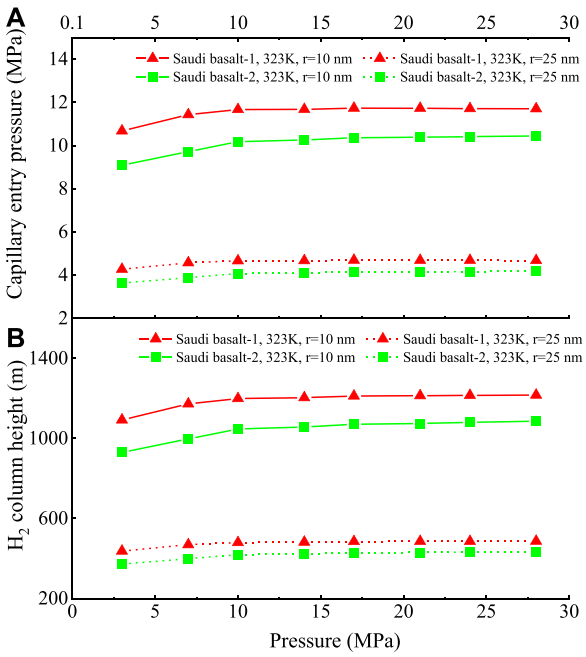

FIGURE 13
The calculated sealing efficiency of H_2/basalt/brine systems versus pressure for Saudi basalts represented by—**(A)** The capillary entry pressure (p_{ce}) and **(B)** the maximum static height of the hydrogen column (h_g^{max}).

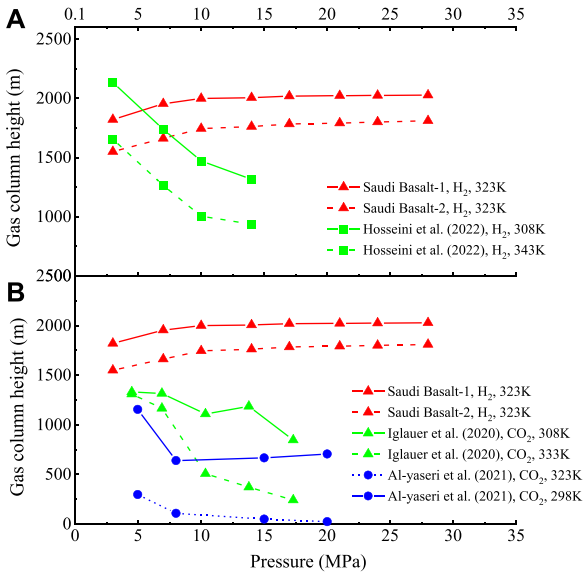

FIGURE 14
The calculated maximum H_2 column heights of the Saudi basalts compared to those of—**(A)** H_2/Iranian basalts by Hosseini et al. (2022a) and **(B)** CO_2/basalts by Iglauer et al. (2020) and Al-Yaseri et al. (2021b).

The capillary entry pressure (p_{ce}) and maximum static gas column height (h_g^{max}) was evaluated using the contact angle measurements and density differences following Eqs 4 and 5, Figures 12A, B. In addition, theoretical pore throat radii values in

the range of 10 and 25 nm were used to evaluate the impact of the pore throat radius on the sample wettability. Basaltic rocks' average pore throat size can range from 6 to 32 nm (Al-Yaseri et al., 2021a; Abdulelah et al., 2021; Hosseini et al., 2022a). The mean pore throat radius of r = 6 nm (Hosseini et al., 2022a) was utilized to calculate the column height for H_2/Iranian basalt and CO_2/Icelandic basalt studies. Thus, the H_2 column height for the Saudi basalts was recalculated using r = 6 nm to present an equivalent comparison. While for the CO_2/WA basalt, r = 29 nm was used as obtained by Al-Yaseri et al. (2021b). The H_2 column height is used to calculate the hydrogen storage capacity or maximum mass of H_2 that can be safely stored in basaltic rock (Shah et al., 2008).

The calculations in this study using H_2/basalt/brine contact angles demonstrate an insignificant influence of pressure on p_{ce} and h_g^{max}, while the pore throat radius demonstrated the highest impact on the sealing efficiency and H_2 storage capacities (Figure 13). The calculated p_{ce} values vary significantly with the pore throat radius with approximately a two-fold decrease in p_{ce} with increasing the pore throat radius from 10 to 25 nm (Figure 13A). The Saudi basalt samples with their pore throat radii less than 10 nm will be able to store a hydrogen column higher than 1,000 m (Figure 13B).

Notably, the p_{ce} in Saudi basalt 1 was always higher than in Saudi basalt 2, consistent with the contact angle measurements, as the elevated hydrogen wettability of Saudi basalt 2 would result in a lower p_{ce}. Moreover, the p_{ce} values of the Saudi basalt samples did not vary significantly with increasing pressure, which can be interpreted as the semi-constant density of H_2 at elevated pressures. The strong water-wet status and less variation in p_{ce} with pressure suggests the good sealing efficiency of Saudi basalt for underground H_2 storage.

The obtained gas column height versus pressure trend of the Saudi basalts varies from that reported in the literature for the H_2/Iranian basalts (Hosseini et al., 2022a) and CO_2/basalts (Iglauer et al., 2020; Al-Yaseri et al., 2021b) (Figures 14A, B). The CO_2/brine/basalt behaviour could be attributed to the sharp increase in CO_2 density with pressure; therefore, a rapidly increasing pressure is expected. On the other hand, we hypothesize that the wide difference in H_2 column height versus pressure between Saudi and Iranian basalts is most likely attributed to their different mineralogy and the presence of some silicate-rich phases (e.g., lizardite) in the Iranian basalt and, therefore, it behaves like clay-rich rocks and become fully-hydrogen wet as pressure increases.

4 Conclusion

- The present study examines the brine wettability of the Saudi basaltic rocks surrounded by H_2 to explore their potential for subsurface H_2 geological storage using the modified form of sessile drop contact angle measurement.
- The Saudi basalt samples are olivine and pyroxene rich with low content of alternation products (e.g., clays).
- The wettability measurements showed that the samples are water-wet. However, the impact of slight variations in mineralogy and surface roughness was paramount in the contact angle measurements.
- The H2/brine/Saudi basalt system showed trends vary significantly from those reported in the literature for CO2/basalt and H2/basalt systems which are attributed to variations in the gas phases as well as the basalt mineralogy.
- The present results demonstrate that pore throat radius has the paramount control on the H2 column height, and the Saudi basalt with average pore throat radii of 10 nm can store more than 1,200 m of H2 column. Moreover, the H2 column did not vary significantly with pressure, which is beneficial for optimal deep geological H2 storage.

Data availability statement

The original contributions presented in the study are included in the article/Supplementary Material, further inquiries can be directed to the corresponding author.

Author contributions

AA: conceptualization, methodology, investigation, data curation, software, and writing—original draft. AA-Y: conceptualization, investigation, formal analysis, writing—review and editing. MM: methodology, validation, resources, and software. ML: conceptualization, validation, formal analysis, writing—review and editing. HH: conceptualization, validation, resources, writing—review and editing, supervision. All authors contributed to the article and approved the submitted version.

Acknowledgments

The authors would like to acknowledge King Abdullah University for Science and Technology (KAUST) for supporting this work by the Research Funding Office under Award No. 4357 and King Fahd University for Petroleum and Minerals (KFUPM) for providing the required infrastructure for this work. The authors would like to thank Jafar Al-Hamad for the fruitful discussion which improved data interpretation and presentation.

Conflict of interest

The authors declare that the research was conducted in the absence of any commercial or financial relationships that could be construed as a potential conflict of interest.

Publisher's note

References

Abdulelah, H., Al-Yaseri, A., Ali, M., Giwelli, A., Negash, B. M., and Sarmadivaleh, M. (2021). CO2/Basalt's interfacial tension and wettability directly from gas density: implications for carbon geo-sequestration. *J. Pet. Sci. Eng.* 204, 108683. doi:10.1016/j.petrol.2021.108683

Abramov, A., Keshavarz, A., and Iglauer, S. (2019). Wettability of fully hydroxylated and alkylated (001) alpha-quartz surface in carbon dioxide atmosphere. *J. Phys. Chem. C* 123, 9027–9040. doi:10.1021/acs.jpcc.9b00263

Aksu, J., Bazilevskaya, E., and Karpyn, Z. (2015). Swelling of clay minerals in unconsolidated porous media and its impact on permeability. *GeoResJ* 7, 1–13. doi:10.1016/j.grj.2015.02.003

Alanazi, A., Ali, M., Bawazeer, S., Yekeen, N., and Hoteit, H. (2022a). Evaluation of cubic, PC-SAFT, and GERG2008 equations of state for accurate calculations of thermophysical properties of hydrogen-blend mixtures. *Energy Rep.* 8, 13876–13899. doi:10.1016/J.EGYR.2022.10.257

Alanazi, A., Ali, M., Mowafi, M., and Hoteit, H. (2022b). "Effect of organics and nanofluids on capillary-sealing efficiency of caprock for hydrogen and carbon-dioxide geological storage," in International Geomechanics Symposium. doi:10.56952/IGS-2022-009

Alanazi, A., Bawazeer, S., Ali, M., Keshavarz, A., and Hoteit, H. (2022c). Thermodynamic modeling of hydrogen-water systems with gas impurity at various conditions using cubic and PC-SAFT equations of state. *Energy Convers. Manag. X* 100257, 100257. doi:10.1016/J.ECMX.2022.100257

Alanazi, A., Baban, A., Ali, M., Keshavarz, A., Iglauer, S., and Hoteit, H. (2023a). Residual trapping of CO2, N2, and a CO2-N2 mixture in Indiana limestone using robust NMR coreflooding: implications for CO2 geological storage. *Fuel* 353, 129221. doi:10.1016/J.FUEL.2023.129221

Alanazi, A., Rasool Abid, H., Usman, M., Ali, M., Keshavarz, A., Vahrenkamp, V., et al. (2023b). Hydrogen, carbon dioxide, and methane adsorption potential on Jordanian organic-rich source rocks: implications for underground H2 storage and retrieval. *Fuel* 346, 128362. doi:10.1016/J.FUEL.2023.128362

Alanazi, A., Yekeen, N., Ali, M., Ali, M., Abu-Mahfouz, I. S., Keshavarz, A., et al. (2023c). Influence of organics and gas mixing on hydrogen/brine and methane/brine wettability using Jordanian oil shale rocks: implications for hydrogen geological storage. *J. Energy Storage* 62, 106865. doi:10.1016/J.EST.2023.106865

Ali, M., Jha, N. K., Pal, N., Keshavarz, A., Hoteit, H., and Sarmadivaleh, M. (2022a). Recent advances in carbon dioxide geological storage, experimental procedures, influencing parameters, and future outlook. *Earth-Science Rev.* 225, 103895. doi:10.1016/J.EARSCIREV.2021.103895

Ali, M., Pan, B., Yekeen, N., Al-Anssari, S., Al-Anazi, A., Keshavarz, A., et al. (2022b). Assessment of wettability and rock-fluid interfacial tension of caprock: implications for hydrogen and carbon dioxide geo-storage. *Int. J. Hydrogen Energy.* 47, 14104–14120. doi:10.1016/J.IJHYDENE.2022.02.149

Al-Mukainah, H., Al-Yaseri, A., Yekeen, N., Hamad, J. A., and Mahmoud, M. (2022). Wettability of shale–brine–H2 system and H2-brine interfacial tension for assessment of the sealing capacities of shale formations during underground hydrogen storage. *Energy Rep.* 8, 8830–8843. doi:10.1016/J.EGYR.2022.07.004

AlRatrout, A., Blunt, M. J., and Bijeljic, B. (2018). Wettability in complex porous materials, the mixed-wet state, and its relationship to surface roughness. *Proc. Natl. Acad. Sci. U. S. A.* 115, 8901–8906. doi:10.1073/pnas.1803734115

Altherr, R., Mertz-Kraus, R., Volker, F., Kreuzer, H., Henjes-Kunst, F., and Lange, U. (2019). Geodynamic setting of upper Miocene to quaternary alkaline basalts from Harrat al 'Uwayrid (NW Saudi Arabia): constraints from K–Ar dating, chemical and Sr-Nd-Pb isotope compositions, and petrological modeling. *Lithos* 330–331, 120–138. doi:10.1016/J.LITHOS.2019.02.007

Al-Yaseri, A., and Jha, N. K. (2021). On hydrogen wettability of basaltic rock. *J. Pet. Sci. Eng.* 200, 108387. doi:10.1016/j.petrol.2021.108387

Al-Yaseri, A. Z., Lebedev, M., Barifcani, A., and Iglauer, S. (2016). Receding and advancing (CO2 + brine + quartz) contact angles as a function of pressure, temperature, surface roughness, salt type and salinity. *J. Chem. Thermodyn.* 93, 416–423. doi:10.1016/J.JCT.2015.07.031

Al-Yaseri, A., Ali, M., Abbasi, G. R., Abid, H. R., and Jha, N. K. (2021a). Enhancing CO2 storage capacity and containment security of basaltic formation using silica nanofluids. *Int. J. Greenh. Gas. Control* 112, 103516. doi:10.1016/J.IJGGC.2021.103516

Al-Yaseri, A., Ali, M., Ali, M., Taheri, R., and Wolff-Boenisch, D. (2021b). Western Australia basalt-CO2-brine wettability at geo-storage conditions. *J. Colloid Interface Sci.* 603, 165–171. doi:10.1016/J.JCIS.2021.06.078

Al-Yaseri, A., Wolff-Boenisch, D., Fauziah, C. A., and Iglauer, S. (2021c). Hydrogen wettability of clays: implications for underground hydrogen storage. *Int. J. Hydrogen Energy* 46, 34356–34361. doi:10.1016/j.ijhydene.2021.07.226

Blunt, M. J. (2016). *Multiphase flow in permeable media, multiphase flow in permeable media*. doi:10.1017/9781316145098

Bui, M., Adjiman, C. S., Bardow, A., Anthony, E. J., Boston, A., Brown, S., et al. (2018). Carbon capture and storage (CCS): the way forward. *Energy Environ. Sci.* 11, 1062–1176. doi:10.1039/C7EE02342A

Cheng, W. M., Xue, J., Zhou, G., Nie, W., and Liu, L. S. (2014). Study of coal dust wettability based on FTIR. *Meitan Xuebao/Journal China Coal Soc.* 39. doi:10.13225/j.cnki.jccs.2013.1715

Chow, Y. T. F., Maitland, G. C., and Trusler, J. P. M. (2018). Interfacial tensions of (H2O + H2) and (H2O + CO2 + H2) systems at temperatures of (298–448) K and pressures up to 45 MPa. *Fluid Phase Equilib.* 475, 37–44. doi:10.1016/J.FLUID.2018.07.022

Coleman, R. G., Gregory, R. T., and Brown, G. F. (1983). Cenozoic volcanic rocks of Saudi Arabia. U.S. Geological Survey. United States Department of the Interior, Geological Survey (Open-File Report 83-788). doi:10.3133/ofr83788

Dake, L. P. (1978). *Fundamentals of Reservoir Engineering*. Elsevier, 443.

Dessert, C., Dupré, B., Gaillardet, J., François, L. M., and Allègre, C. J. (2003). Basalt weathering laws and the impact of basalt weathering on the global carbon cycle. *Chem. Geol.* 202, 257–273. doi:10.1016/j.chemgeo.2002.10.001

Duncan, R. A., and Al-Amri, A. M. (2013). Timing and composition of volcanic activity at Harrat Lunayyir, western Saudi Arabia. *J. Volcanol. Geotherm. Res.* 260, 103–116. doi:10.1016/J.JVOLGEORES.2013.05.006

Espinoza, N., and Santamarina, J. C. (2017). CO2 breakthrough—caprock sealing efficiency and integrity for carbon geological storage. *Int. J. Greenh. Gas. Control* 66, 218–229. doi:10.1016/J.IJGGC.2017.09.019

Gadelmawla, E. S., Koura, M. M., Maksoud, T. M. A., Elewa, I. M., and Soliman, H. H. (2002). Roughness parameters. *J. Mater. Process. Technol.* 123, 133–145. doi:10.1016/S0924-0136(02)00060-2

Gislason, S. R., and Oelkers, E. H. (2014). Carbon storage in basalt. *Science (80-.)* 344, 373–374. doi:10.1126/science.1250828

Gislason, S. R., Wolff-Boenisch, D., Stefansson, A., Oelkers, E. H., Gunnlaugsson, E., Sigurdardottir, H., et al. (2010). Mineral sequestration of carbon dioxide in basalt: A pre-injection overview of the CarbFix project. *Int. J. Greenh. Gas. Control* 4, 537–545. doi:10.1016/j.ijggc.2009.11.013

Harnois, L. (1988). The CIW index: A new chemical index of weathering. *Sediment. Geol.* 55, 319–322. doi:10.1016/0037-0738(88)90137-6

Hashemi, L., Glerum, W., Farajzadeh, R., and Hajibeygi, H. (2021). Contact angle measurement for hydrogen/brine/sandstone system using captive-bubble method relevant for underground hydrogen storage. *Adv. Water Resour.* 154, 103964. doi:10.1016/J.ADVWATRES.2021.103964

Heinemann, N., Alcalde, J., Miocic, J. M., Hangx, S. J. T., Kallmeyer, J., Ostertag-Henning, C., et al. (2021). Enabling large-scale hydrogen storage in porous media – The scientific challenges. *Energy Environ. Sci.* 14, 853–864. doi:10.1039/D0EE03536J

Hosseini, M., Ali, M., Fahimpour, J., Keshavarz, A., and Iglauer, S. (2022a). Basalt-H2-brine wettability at geo-storage conditions: implication for hydrogen storage in basaltic formations. *J. Energy Storage* 52, 104745. doi:10.1016/J.EST.2022.104745

Hosseini, M., Ali, M., Fahimpour, J., Keshavarz, A., and Iglauer, S. (2022b). Assessment of rock-hydrogen and rock-water interfacial tension in shale, evaporite and basaltic rocks. *J. Nat. Gas. Sci. Eng.* 106, 104743. doi:10.1016/J.JNGSE.2022.104743

Hosseini, M., Fahimpour, J., Ali, M., Keshavarz, A., and Iglauer, S. (2022c). Capillary sealing efficiency analysis of caprocks: implication for hydrogen geological storage. *Energy and Fuels acs.energyfuels.2c00281* 36, 4065–4075. doi:10.1021/ACS.ENERGYFUELS.2C00281

IEA (2018). World energy outlook 2018: highlights. *Int. Energy Agency* 1, 643.

Iglauer, S., Al-Yaseri, A. Z., and Wolff-Boenisch, D. (2020). Basalt-CO2-brine wettability at storage conditions in basaltic formations. *Int. J. Greenh. Gas. Control* 102, 103148. doi:10.1016/J.IJGGC.2020.103148

Iglauer, S. (2022). Optimum geological storage depths for structural H2 geo-storage. *J. Pet. Sci. Eng.* 212, 109498. doi:10.1016/j.petrol.2021.109498

Jiu, B., Huang, W., Li, Y., and He, M. (2021). Influence of clay minerals and cementation on pore throat of tight sandstone gas reservoir in the eastern Ordos Basin, China. *J. Nat. Gas Sci. Eng.* 87, 103762.

Johnson, R. E., and Dettre, R. H., 1964. Contact angle hysteresis. doi:10.1021/ba-1964-0043.ch007

Kaliwoda, M., Altherr, R., and Meyer, H. P. (2007). Composition and thermal evolution of the lithospheric mantle beneath the Harrat Uwayrid, eastern flank of the Red Sea rift (Saudi Arabia). *Lithos* 99, 105–120. doi:10.1016/j.lithos.2007.06.013

Kanaani, M., Sedaee, B., and Asadian-Pakfar, M. (2022). Role of cushion gas on underground hydrogen storage in depleted oil reservoirs. *J. Energy Storage* 45, 103783. doi:10.1016/j.est.2021.103783

Kwok, D. Y., and Neumann, A. W. (1999). Contact angle measurement and contact angle interpretation. *Adv. Colloid Interface Sci.* 81, 167–249. doi:10.1016/S0001-8686(98)00087-6

Lander, L. M., Siewierski, L. M., Britain, W. J., and Vogler, E. A. (1993). A systematic comparison of contact angle methods. *Langmuir* 9, 2237–2239. doi:10.1021/la00032a055

Leila, M., Moscariello, A., and Šegvić, B. (2018). Geochemical constraints on the provenance and depositional environment of the messinian sediments, onshore nile

delta, Egypt: implications for the late Miocene paleogeography of the mediterranean. *J. Afr. Earth Sci.* 143, 215–241. doi:10.1016/j.jafrearsci.2018.03.024

Leila, M., Levy, D., Battani, A., Piccardi, L., Segvic, B., Badurina, L., et al. (2021). Origin of continuous hydrogen flux in gas manifestations at the Larderello geothermal field, Central Italy. *Chem. Geol.* 585, 120564. doi:10.1016/j.chemgeo.2021.120564

Leila, M., Loisseau, K., and Moretti, I. (2022). Controls on generation and accumulation of blended gases (CH4/H2/He) in the Neoproterozoic Amadeus Basin, Australia. *Mar. Pet. Geol.* 140, 105643. doi:10.1016/j.marpetgeo.2022.105643

Lemmon, E. W., Bell, I. H., Huber, M. L., and McLinden, M. O. (2018). *NIST Standard Reference Database 23: Reference Fluid Thermodynamic and Transport Properties—REFPROP, Version 10.0*. Gaithersburg, MD: National Institute of Standards and Technology, Standard Reference Data Program.

Li, D., and Neumann, A. W. (1992). Equation of state for interfacial tensions of solid-liquid systems. *Adv. Colloid Interface Sci.* 39, 299–345. doi:10.1016/0001-8686(92)80064-5

Li, M., Bussonnière, A., Xiang, B., Manica, R., and Liu, Q. (2022). Effect of solid wettability on three-phase hydrodynamic cavitation. *Min. Eng.* 180, 107455. doi:10.1016/j.mineng.2022.107455

Liang, X., Zhou, F., Liang, T., Su, H., Yuan, S., and Li, Y. (2020). Impacts of pore structure and wettability on distribution of residual fossil hydrogen energy after imbibition. *Int. J. Hydrogen Energy* 45, 14779–14789. doi:10.1016/J.IJHYDENE.2020.03.208

Liu, H., Luo, B., Shen, S., and Li, L. (2019). Design and mechanical tests of basalt fiber cloth with MAH grafted reinforced bamboo and poplar veneer composite. *Eur. J. Wood Wood Prod.* 77, 271–278. doi:10.1007/s00107-018-1378-9

Ma, J., Li, Q., Kempka, T., and Kühn, M. (2019). Hydromechanical response and impact of gas mixing behavior in subsurface CH4 Storage with CO2-based cushion gas. *Energy Fuels* 33, 6527–6541. doi:10.1021/acs.energyfuels.9b00518

Madhurima, V., Purkayastha, D. D., and Rao, N. V. S. (2011). Wettability, FTIR and dielectric studies of 1,4-dioxane and water system. *J. Colloid Interface Sci.* 357, 229–233. doi:10.1016/j.jcis.2011.01.090

Matter, J. M., Stute, M., Snæbjörnsdottir, S., Oelkers, E. H., Gislason, S. R., Aradottir, E. S., et al. (2016). Rapid carbon mineralization for permanent disposal of anthropogenic carbon dioxide emissions. *Sci. (80-.)* 352, 1312–1314. doi:10.1126/science.aad8132

Mbonyiryivuze, A., Mwakikunga, B., Dhlamini, S. M., Maaza, M., Mokhotjwa Dhlamini, S., Park, E., et al. (2015). Morphological and chemical composition characterization of commercial sepia melanin. *Phys. Mater. Chem.* 3, 22–27. doi:10.12691/ajn-3-1-3

McCollom, T., and Bach, W. (2009). Thermodynamic constraints on hydrogen generation during serpentinization of ultramafic rocks. *Geochim. Cosmochim. Acta* 73, 856–875. doi:10.1016/j.gca.2008.10.032

Mehmani, A., Kelly, S., Torres-Verdín, C., and Balhoff, M. (2019). Capillary trapping following imbibition in porous media: microfluidic quantification of the impact of pore-scale surface roughness. *Water Resour. Res.* 55, 9905–9925. doi:10.1029/2019WR025170

Michalski, J., Bünger, U., Crotogino, F., Donadei, S., Schneider, G., Pregger, T., et al. (2017). Hydrogen generation by electrolysis and storage in salt caverns: potentials, economics and systems aspects with regard to the German energy transition.

Morrow, N. R. (1975). Effects of surface roughness on contact angle with special reference to petroleum recovery. *J. Can. Pet. Technol.* 14, 42–53. doi:10.2118/75-04-04/2166536/PETSOC-75-04-04.PDF/1

Oh, T., and Choi, C. K. (2010). Comparison between SiOC thin film by plasma enhance chemical vapor deposition and SiO2 thin film by fourier Transform infrared spectroscopy. *J. Korean Phys. Soc.* 56, 1150–1155. doi:10.3938/jkps.56.1150

Pan, B., Yin, X., Ju, Y., and Iglauer, S. (2021). Underground hydrogen storage: influencing parameters and future outlook. *Adv. Colloid Interface Sci.* 294, 102473. doi:10.1016/j.cis.2021.102473

Pfeiffer, W. T., Beyer, C., and Bauer, S. (2017). Hydrogen storage in a heterogeneous sandstone formation: dimensioning and induced hydraulic effects. *Pet. Geosci.* 23, 315–326. doi:10.1144/petgeo2016-050

Pillai, P., Kumar, A., and Mandal, A. (2018). Mechanistic studies of enhanced oil recovery by imidazolium-based ionic liquids as novel surfactants. *J. Ind. Eng. Chem.* 63, 262–274. doi:10.1016/j.jiec.2018.02.024

Prinzhofer, A., Cissé, C., and Diallo, A. (2018). Discovery of a large accumulation of natural hydrogen in Bourakebougou (Mali). *Int. J. Hydrog. Energy* 43, 19315–19326. doi:10.1016/j.ijhydene.2018.08.193

Rucker, M., Naderi, M., Yesufu-Rufai, S., Lowe, S., Marcelis, F., Rayan, M., et al. (2019). *Impact of texture and mineralogy on the wettability of rock surfaces*. AGU fall meetings. Abstracts.

Shah, V., Broseta, D., Mouronval, G., and Montel, F. (2008). Water/acid gas interfacial tensions and their impact on acid gas geological storage. *Int. J. Greenh. Gas. Control* 2, 594–604. doi:10.1016/j.ijggc.2008.02.002

Tadmor, R. (2004). Line energy and the relation between advancing, receding, and Young contact angles. *Langmuir* 20, 7659–7664. doi:10.1021/la049410h

Tarkowski, R. (2019). Underground hydrogen storage: characteristics and prospects. *Renew. Sustain. Energy Rev.* 105, 86–94. doi:10.1016/j.rser.2019.01.051

Waman, V. S., Funde, A. M., Kamble, M. M., Pramod, M. R., Hawaldar, R. R., Amalnerkar, D. P., et al. (2011). Hydrogenated nanocrystalline silicon thin films prepared by hot-wire method with varied process pressure. *J. Nanotechnol.* 2011, 1–10. doi:10.1155/2011/242398

Weltje, G. J., Meijer, X. D., and De Boer, P. L. (1998). Stratigraphic inversion of siliciclastic basin fills: A note on the distinction between supply signals resulting from tectonic and climatic forcing. *Basin Res.* 10, 129–153. doi:10.1046/j.1365-2117.1998.00057.x

White, S. K., Spane, F. A., Schaef, H. T., Miller, Q. R. S., White, M. D., Horner, J. A., et al. (2020). Quantification of CO2Mineralization at the wallula basalt pilot project. *Environ. Sci. Technol.* 54, 14609–14616. doi:10.1021/ACS.EST.0C05142

Yekeen, N., Padmanabhan, E., Abdulelah, H., Irfan, S. A., Okunade, O. A., Khan, J. A., et al. (2021). CO2/brine interfacial tension and rock wettability at reservoir conditions: A critical review of previous studies and case study of black shale from Malaysian formation. *J. Pet. Sci. Eng.* 196, 107673. doi:10.1016/j.petrol.2020.107673

Yekta, A. E., Manceau, J.-C. C., Gaboreau, S., Pichavant, M., and Audigane, P. (2018). Determination of hydrogen–water relative permeability and capillary pressure in sandstone: application to underground hydrogen injection in sedimentary formations. *Transp. Porous Media* 122, 333–356. doi:10.1007/S11242-018-1004-7

Yen, T. H. (2015). Effects of wettability and interfacial nanobubbles on flow through structured nanochannels: an investigation of molecular dynamics. *Mol. Phys.* 113, 3783–3795. doi:10.1080/00268976.2015.1062928